Journal of the European Ceramic Society 21 (2001) 833–840

www.elsevier.com/locate/jeurceramsoc

Microstructure and creep behavior of an Y-α-β sialon composite

M.T. Lin, J.L. Shi *, L. Wang, D.Y. Jiang, M.L. Ruan, T.R. Lai

The State Key Lab of High Performance Ceramics and Superfine Microstructure, Shanghai Institute of Ceramics, Chinese Academy of Sciences, Shanghai 200050, People's Republic of China

Received 15 June 2000; received in revised form 4 September 2000; accepted 10 September 2000

Abstract

Flexural creep behavior of a Y-α-β sialon composite was studied in air at temperatures of 1250–1350°C and stresses of 110–290 MPa. The composite in which YAG was designed as intergranular phase has an original α/β ratio of 65/35. The stress exponents in Norton equation were determined to be 1.31±0.12, 1.49±0.15 and 1.62±0.10 at 1250, 1300 and 1350°C, respectively, and creep activation energy was 677±25 kJ mol^{-1}. Combining the microstructure observations, grain boundary diffusion accommodated by grain boundary sliding was identified as the rate-controlling creep mechanism for the composite. The creep rate exponent p in Monkman–Grant relation was found to be 1.6, and the nucleation and growth of cavities in triple grain pockets was responsible for the creep rupture.

Keywords: Creep; Microstrusture-final; Oxidation; Phase transformations; Sialons

1. Introduction

Sialon ceramics are members of Si_3N_4-based ceramic family with excellent properties, such as high strength, high hardness, low thermal expansion, good creep resistance and oxidization resistance. Because of their potential use in hot ceramic engines, sialon ceramics have been intensively investigated for several decades. High temperature properties, especially high temperature creep resistance, will finally determine their being used as components of ceramic engines. Several measures have been taken by scientists to improve the high temperature mechanical properties of sialon ceramics, including: (1) Preparing highly pure starting powders; (2) developing advanced sintering processes, e.g. hot press (HP), hot isostatical press (HIP) and reaction bonded sintering (RB); (3) introducing second phase materials into sialon matrix, which mainly are nanoparticles, whiskers, fibers and platelets; (4) tailoring the microstructure of sialon ceramics; (5) seeking high melt point and highly refractory intergranular phases.

Y-α-β sialon composite is a product through the above properties designing. Y-α sialon, with a formula of $Y_{m/3}Si_{12-m-n}Al_{m+n}O_nN_{16-m-n}$, has higher hardness; β sialon, with a formula of $Si_{6-z}Al_zO_zN_{8-z}$, has higher strength and toughness. Sialon ceramics have both advantages of Y-α sialon and β sialon can be achieved via designing α/β sialon composite with a certain α/β ratio. Meanwhile, nowadays liquid sintering method is widely employed in the sintering of sialon ceramics through the introduction of additives; glassy or crystalline intergranular phases are inevitably introduced between sialon grains, which dominate the high temperature properties of sialon ceramics.[1] For Y-α-β sialon composite, additives Y_2O_3, Al_2O_3 and AlN were introduced. Part of these additives enter the lattice of Si_3N_4 to form the solutions α sialon and β sialon, the others present at grain boundaries as Y–Si–Al–O–N glass and crystalline YAG. At present, YAG is recognized as the best intergranular phase for sialon ceramics.[2]

Good creep resistance for sialon ceramics is essential for their final application. Since 1970s, the creep data of Si_3N_4 or Si_3N_4-based ceramics prepared by various processes has been seen in a large body of literature. Creep behavior of sialon ceramics has also been extensively studied.[3–10] Previous work has shown that the creep behavior of sialon or Si_3N_4 ceramics involves mechanisms of grain boundary sliding, solution/precipitation, diffusion, viscous flow and cavities,[11] and the nucleation/growth, coalescence and linkage of cavities are responsible for the creep rupture of sialon ceramics.[11–14]

* Corresponding author. Tel.: +86-21-6251-2990-5166; fax: +86-21-6251-13903.

E-mail address: jlshi@sunm.shcnc.ac.cn (J.L. Shi).

0955-2219/01/$ - see front matter
PII: S0955-2219(00)00269-7

In this paper, high-temperature creep behavior for a Y-α-β sialon composite with an original α/β ratio of 65/35 were investigated. Stress exponents at several temperatures and the creep activation energy were determined, combining the microstructure observations and XRD analysis, the rate-controlling mechanism for creep was elucidated. The effect of oxidation and phase transformation on creep behavior of the composite was also interpreted.

2. Experiment procedure

The starting materials were Si_3N_4 76.03 wt.%, Al_2O_3 5.02 wt.%, AlN 12.39 wt.% and Y_2O_3 6.56 wt.%. Si_3N_4 was from UBE with grade SN-E10, the others were local products of high purity (> 99.9 wt.%). The powders were mixed in alcohol and milled in a plastic jar with sialon balls as milling media. After drying, the batch was sieved and packed into a graphite die and sintered at a temperature of 1800°C and a load of 24 MPa for an hour in N_2 atmosphere, discs of 70 mm diameter were prepared. Then the discs were machined into testing bars with dimensions of $2\times4\times40$ mm^3. Before creep, the samples were annealed at 1350°C for 24 h in N_2 atmosphere. XRD of the as-heat-treated samples revealed that the sialon composite had an original α/β sialon ratio of 65/35 ($z=0.75$ for β sialon, $m=1.0$ and $n=1.5$ for a sialon) and YAG/(α + β) ratio of 3.1%. The density, determined by Archimedes' principle in distilled water, was 3.268 g cm^{-3}.

The samples were crept on four-point bending creep apparatus with a cantilever of 8:1, and the fixture was made of highly pure SiC with outer and inner span of 30 and 10 mm, respectively. Molybdenum disilicate element was used to heat the furnace and a Pt/Pt_{10}-Rh thermocouple was used to monitor the temperature through a programmable controller which offered ±2°C temperature control. The nominal applied stress and creep strain were the stress and strain of the outer fiber surface of the creep specimen, which were calculated by a method similar to that used by Cannon et al.[15] The central deflection of the outer fiber surface of the creep sample was measured by an extensometer consisted of a ruby probe which was connected to a linear-variable differential transducer (LVDT) with an accuracy of ±1 μm. The LVDT was connected to a personnel computer which continuously recorded the deflection data through a digital displacement meter. The room temperature was controlled to about 22°C, using an air conditioner (CS-5BHII, National, Japan). Before loading, the system was held at given temperature for half an hour to minimize the instability of temperature. The stress exponents and creep activation energy were obtained according to the following equation:

$$\dot{\varepsilon}_s = A\sigma^n \exp(-Q/RT) \quad (1)$$

where $\dot{\varepsilon}_s$ is the steady-state creep rate, A a pre-exponential factor depending on the material structure, α the applied stress, n the stress exponent, Q the creep activation energy, and RT has usual meaning. More than 10 samples were used for tests. In order to minimize the influence of the change of microstructure and composition on the determination of stress exponents and creep activation energy, stress exponents and creep activation energy were determined by stress jump method and temperature jump method, respectively.

The microstructure of the as-heat-treated and crept samples were studied by transmission electron microscopy (TEM) and high resolution electron microscopy (HREM, JEM-2010, JEOL corporation, Japan, theoretical resolution 0.14 nm) with energy dispersive spectrascopy (EDS, LINKISIS) at both micrometer and nanometer scale. The morphologies of oxidation scales were analyzed by scanning electron microscopy (SEM, EPMA-8705QHII). Samples for TEM and HREM analysis were taken from the tensile side of the crept sample. Grain sizes of mat-erials were estimated by an intercept method used by Shi et al.[16] The contents of α sialon, β sialon and YAG were calculated from XRD results using the reflection peak strength of α_{210}, β_{210}, α_{102} and YAG_{420}.[17]

3. Results

3.1. Creep behavior

Creep data are presented in Fig. 1(a)–(e). Creep curves at single temperature and stress in Fig. 1(a) show that the strain–time curves consist of transient state region of about 3–20 h during which creep rates decrease continuously as time increases, followed by a quasi-steady state region with creep rate in the range of 10^{-9}–10^{-7} s^{-1}. No accelerated creep was observed before the failure of the samples. The highest creep strain at rupture is about 0.7%, strongly depending on testing conditions, especially temperature. Data in Fig. 1(b)–(e) were used to calculate the stress exponents and creep activation energy in Eq. (1).

At temperatures of 1250, 1300 and 1350°C, apparently linear fitting of the log(creep rate)–log(applied stress) plots according to the data in Fig. 1(b)–(d), give stress exponents 1.31±0.12, 1.45±0.15 and 1.62±0.10, respectively, which are in good agreement with the results that were reported by other authors[18–21] for Y_2O_3 and/or Al_2O_3 doped Si_3N_4. One major discrepancy is that the intergranular phases in our material are partly crystalline YAG, while those in other authors materials are all Y–Si–Al–O–N glass.

The Arrhenius plot between creep rate and temperature based on the data in Fig. 1(e) gives the creep activation

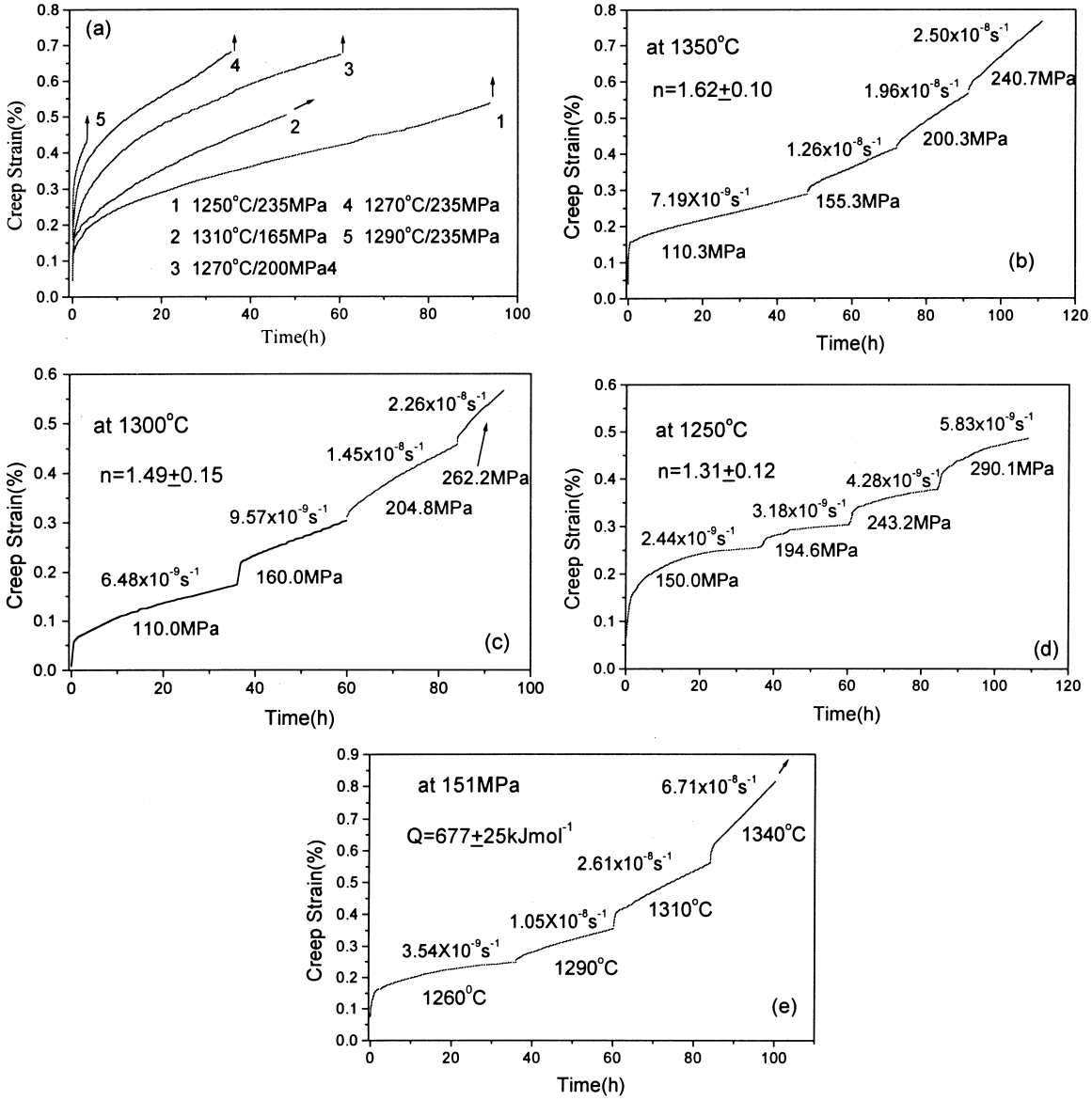

Fig. 1. Bending–creep curves: (a) by single temperature and stress; (b–e) by stepwise method.

energy of 677±25 kJ mol^{-1}, which agrees reasonably well with those reported by Xu et al.[20] in the creep of YL2 and Todd and Xu[19] for Si_3N_4–$6Y_2O_3$–$2Al_2O_3$, but, much higher than the value of SNY given by Šajgalik et al.[18]

3.2. Microstructure

Fig. 2 shows the microstructure of as-heat-treated samples. Y-α sialon grains are equiaxed with grain sizes 0.2–1.5 μm, β sialon grains are acicular with an aspect ratio greater than 5.

TEM micrographs of the sample crept at 1250°C and 235 MPa in Fig. 3 reveal that almost all cavities are wedged-shaped ones with round corners. This observation implies that grain boundary sliding is an important factor for initiation of cavities during creep deformation. XRD results of the crept sample [as shown in Fig. 4(b)] indicate that the content of intergranular phase YAG increases from 3.1 to 7.4%, and β/α+β ratio decreases from 35 to 25%, comparing to the as-heat-treated sample [as shown in Fig. 4(a)]. According to the HREM micrographs of the crept sample in Fig. 5, no obvious discrepancy between the thickness of β/α grain boundaries and that of β/β grain boundaries was found, the grain boundary thickness is about 0.6–0.8 nm, which falls in the range of 0.5–1.0 nm as observed for most Si_3N_4 ceramics. The intergranular phases at two grain boundary mainly are Y–Si–Al–O–N glass, and those at triple grain junctions are Y–Si–Al–O–N glass and YAG crystalline. A few dislocations were also found in elongated β sialon grains.

SEM micrographs of the oxidation scales for the sample crept at 1250°C and 235 MPa are shown in Fig. 6. Fig. 6(a) shows the surface of the oxidation scale.

N_2 pores in the range of 4–16 μm diameter and $Y_2Si_2O_7$ grains, with rectangular shape and preferential orientation, disperse in the Y–Si–Al–O–N glass scales inhomogeneously. Fig. 6(b) and (c) show the thickness of the oxidation scales (about 10–25 μm) at the tensile side and compressive side, respectively.

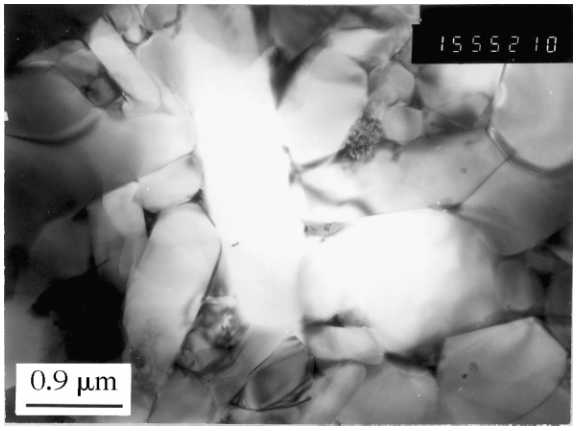

Fig. 2. TEM micrographs of the as-heat-treated sample.

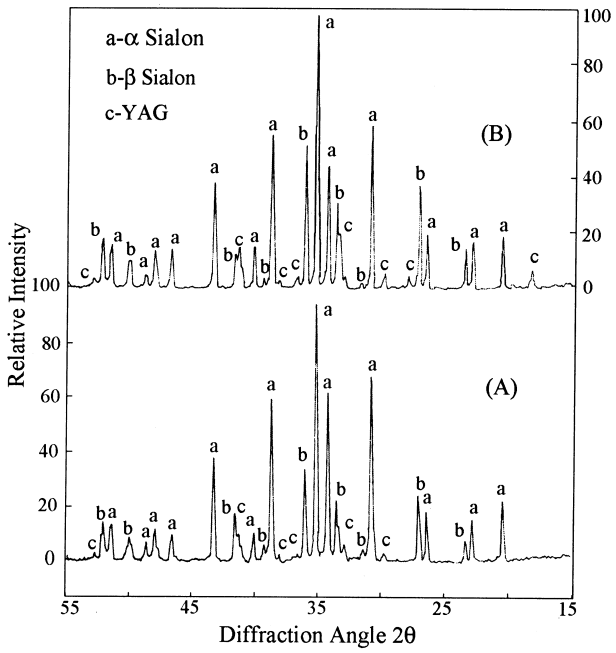

Fig. 4. XRD patterns for (A) the virgin sample and (B) the crept sample the same as that for Fig. 3.

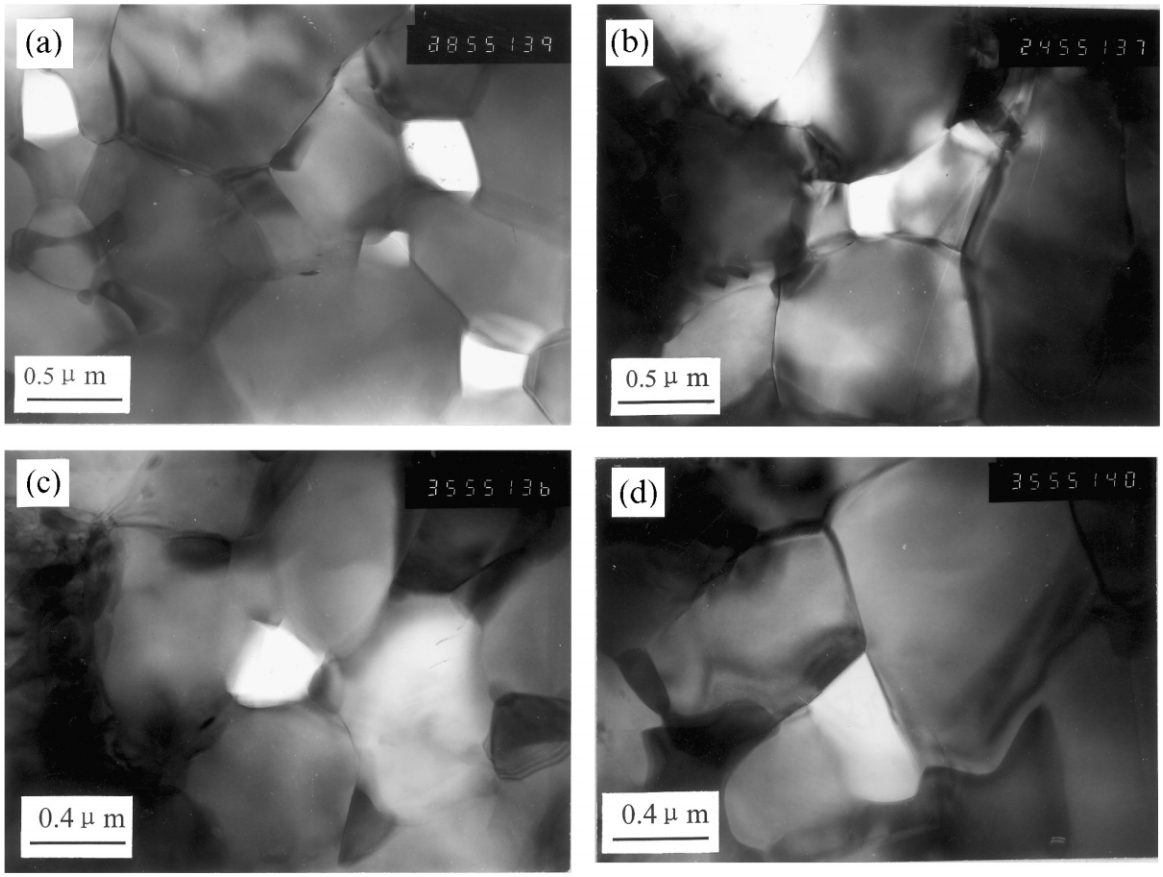

Fig. 3. TEM micrographs of the sample crept for 94 h at 1250°C and 235 MPa with a creep strain of 0.5%, showing at triple grain junctions the cavities found.

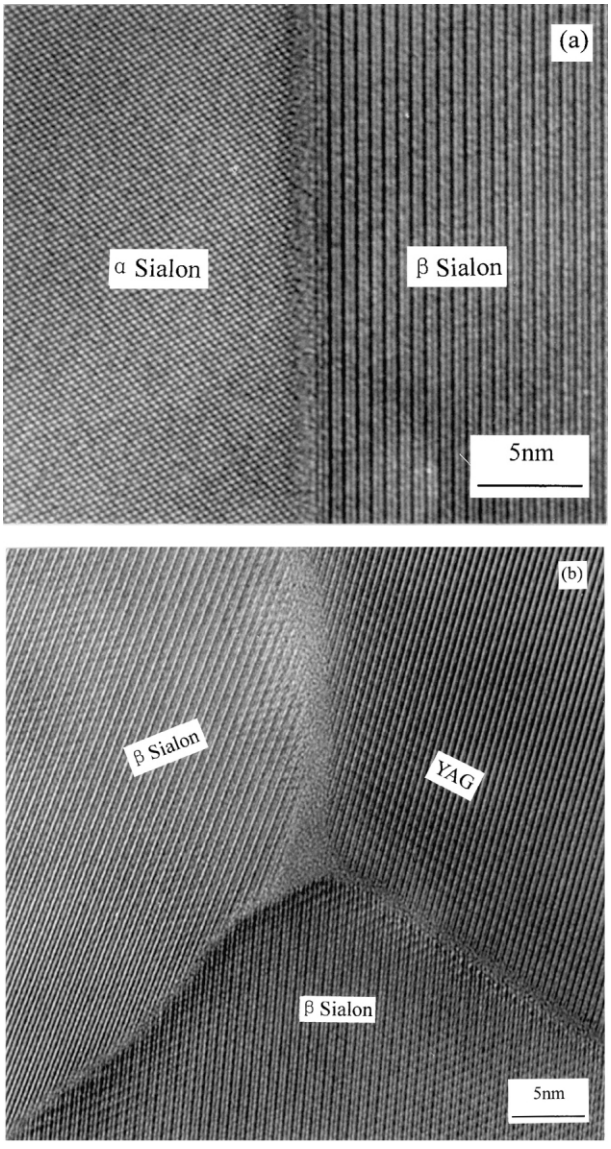

Fig. 5. HREM of the crept sample the same as that for Fig. 3, showing: (a) α/β and (b) β/β grain boundaries.

4. Discussions

4.1. Creep mechanisms

Creep tests of sialon ceramics are aimed to unveil the creep deformation mechanisms, which provide direct evidence for their reliability evaluation. At present, the creep mechanisms are identified by three parameters: stress exponent, activation energy and microstructure change, in which the stress exponent is the most important parameter.

In Chokshi and Langdon's review[22] on creep mechanisms of ceramics, the creep deformation with stress exponents 1–3 is attributed to grain boundary sliding, diffusion, interface reaction and cavities, creep deformation with stress exponent greater than 3 is attributed to the motion of intragranular dislocations. For sialon ceramics, which are usually deformed at temperature below 1700°C, the dislocations are difficult to be activated because of high Peierls force, therefore, in this paper, dislocation is too low in density to be a major creep mechanism. In the present experiment, the stress exponents of 1.3∼4.6 fall in the range of 1∼3 for most previous work on the creep of Si_3N_4-based ceramics,[19] we believe that grain boundary diffusion is a dominant creep mechanism for the sialon composite. This inference is similar to those made by Xu et al.[20] and Todd and Xu[19] for Y_2O_3 and Al_2O_3 doped Si_3N_4. Xu et al. suggested a diffusion-grain boundary sliding mechanism, and Todd and Xu assumed that grain boundary diffusion accompanied by the formation of wedge-shaped cavities was the dominant creep mechanism.

Creep activation energy provides interesting details of creep mechanisms, although it can not act as criteria for the identification of creep mechanisms. Most creep activation energies of Si_3N_4 ceramics fall in the range 650–750 kJ mol^{-1},[19,23,24] which involve the creep mechanisms of grain boundary sliding and solution–diffusion–precipitation. In our experiment, the creep activation energy is 677 kJ mol^{-1}, higher than the activation energy of 546–630 kJ mol^{-1} for the solution–precipitation mechanism of nitrogen ceramics,[25] which indicates that the solution–precipitation is not the rate controlling mechanism for the sialon composite.

Microstructure observations show microstructure changes during creep, such as the formation of cavities, strain whorls, the change of grain morphologies and devitrification of intergranular phases. These information are useful evidences for the identification of rate-controlling creep mechanisms. TEM observations in Fig. 3 show, only on triple grain junctions, the cavities were found. These observations provide powerful evidence for grain boundary sliding.

So far, we can draw the conclusion that diffusion coupled with grain boundary sliding is the dominant creep mechanism for the creep of the sialon composite. For this creep deformation mechanism, Stevens gave the quantitative analysis[26] that, under small creep strain condition, grain boundary sliding has the same contribution to the total creep strain as diffusion.

For the sialon composite crept at 1250, 1300 and 1350°C, the stress exponents are 1.31, 1.49 and 1.62, respectively. This observation, i.e. the values of stress exponents decrease as the temperature decreases, can be attributed to cavities at mutli grain junctions, cavities can increase the value of creep exponent.[27,28] At lower temperatures, the higher viscosity of intergranular glass increases the energy barrier for grain boundary sliding and diffusion, and inhibits the formation of wedge-shaped cavities.

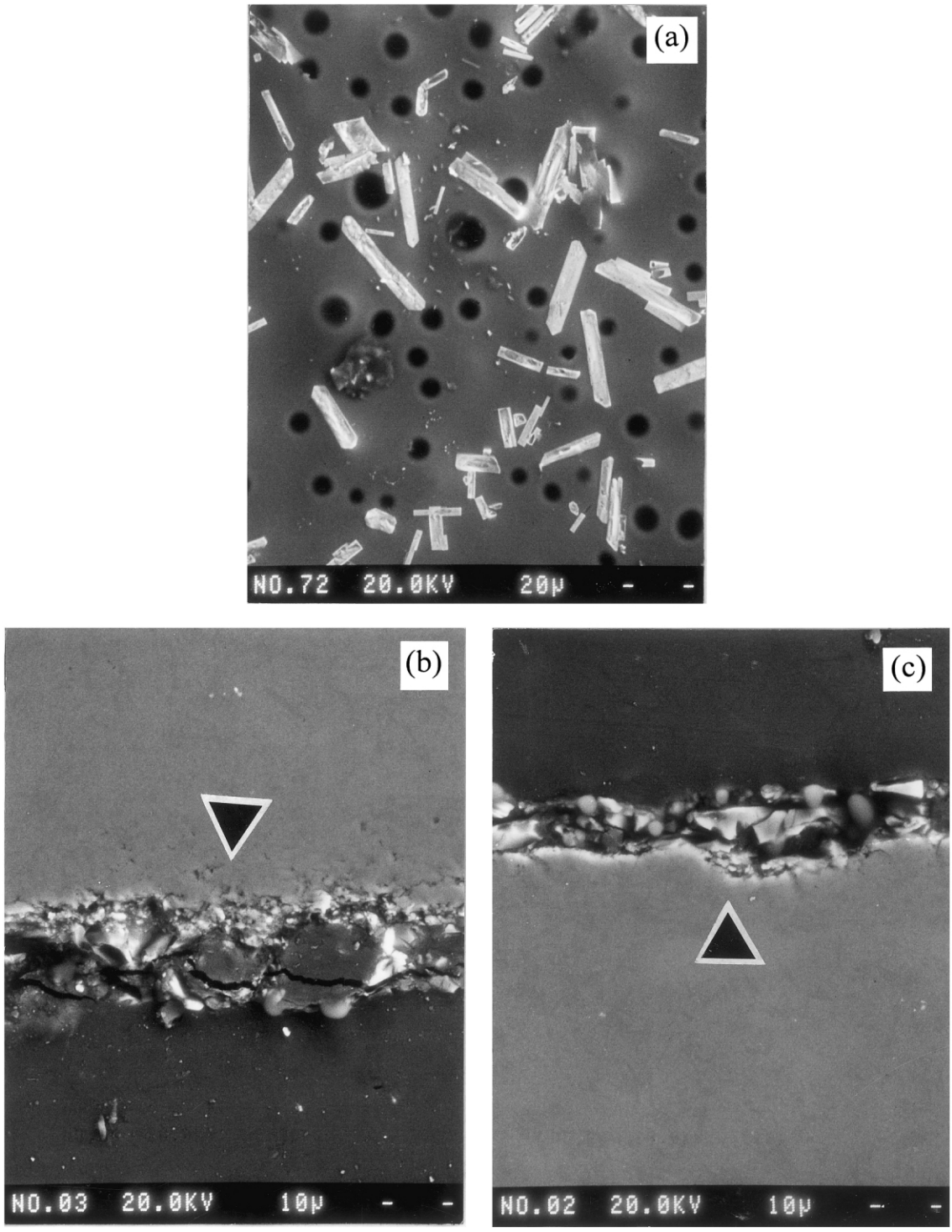

Fig. 6. SEM micrographs of the crept sample identical to that for Figs. 3–5, showing: (a) the surface of the oxidation scale, (b) thickness of the oxidation scale on the tensile side and (c) thickness of the oxidation scale on the compressive side.

4.2. Time to fracture

Si_3N_4-based ceramics being used at high temperature are mainly damaged by creep rupture. Creep rupture is the result of the continuous nucleation and growth of cavities at grain boundaries and triple grain junctions. According to Evans and Rana's statistical model[29] for high temperature rupture in ceramics, cavities initiate primarily near triple junctions for ceramics containing glassy intergranular phase. Under the applied stress, wedge-shape cavities are formed because a small amount of glass with high viscosity are not enough to fill the

triple junctions by diffusional or viscous flow during grain boundary sliding. This is why only wedge-shaped cavities were observed in our experiment.

A small amount of glassy intergranular phase can dominate the creep rupture,[30] via the formation of microcracks at triple grain junctions. In this paper, the liquid film in two grain junctions promote the grain boundary sliding, while the wedge-shaped cavities are formed at triple grain junctions due to the tensile stress.

The Monkman–Grant relation[31] is the most popular creep rupture model, which describes a power law relation between creep rupture time and steady creep rate, i.e.

$$t_f \varepsilon_s^p = C \tag{2}$$

where t_f is the time to failure, $\dot{\varepsilon}_s$ is the steady creep rate, p is creep rate exponent, and C is a constant. According to the failure data in Fig. 1(a), the value p was calculated to be 1.6.

4.3. The effect of oxidation on creep

For several decades, much work has been focused on the oxidation of sialon or Si_3N_4 ceramics by both ways of thermodynamics and kinetics,[32–37] but the real oxidation mechanisms have not been well interpreted, for instance, there is still an argument on the existence of N–O scale between the bulk and the oxidation layer.[36] However, the parabolic law,[37] i.e.

$$\left(\frac{w}{A}\right)^2 = kt \tag{3}$$

has been commonly accepted, where w is weight gain, A the surface area of the sample, k rate constant and t time. oxidization activation energy estimated from the above equation is 741 kJ mol^{-1}, approaching to the creep activation energy, 677 kJ mol^{-1}, which indicates that oxidation has almost the same rate controlling mechanism as creep.

Due to the different microstructure and composition, Y-α sialon is more oxidation resistant than β sialon. This phenomenon can be further confirmed by the fact that the magnitude of the self diffusion coefficient of N^3 for single α Si_3N_4 grain is around one order lower than that for single β Si_3N_4 grain at the same temperature.[38] Non-catastrophic oxidation enhances the creep resistance.[24] As Lewis and Barnard pointed out,[32] during oxidation, a passive oxidation scale is formed on the sample surface, which fills the cracks and cavities and releases the stress concentration, the intergranular phase becomes purified and thinner and the bonding energy between sialon grains increases. According to the following reaction[36]

$$Si_{5.25}Al_{0.75}O_{0.75}N_{7.25} + 5.44O_2 \rightarrow 5.25SiO_2 + 0.375Al_2O_3 + 3.625N_2 \tag{4}$$

$$Y_{0.33}Si_{9.5}Al_{2.5}O_{1.5}N_{13.5} + 10.90O_2 \rightarrow 8.32SiO_2 + 0.17Y_2Si_2O_7 + 0.42Al_6Si_2O_{13} + 6.75N_2 \tag{5}$$

Oxidation of the two sialons proceeds via N^{3-} transferring its charge to O_2. The diffusion of N^{3-} or N^{3-} and Y^{3+} complex species is assumed to be the rate controlling mechanism for sialon oxidation.[10,19]

4.4. Phase transformation during creep

XRD of crept samples reveals that considerable phase transformation happens during creep with the increase of the content of intergranular phase YAG, e.g. for the sample crept at 1250°C and 235 MPa, the content of YAG is 7.4 wt.% comparing to 3.1 wt.% for the as-heat-treated sample. Phase transformation occurs more quickly at higher temperature. However, the mechanism of transformation has not been very clear.[39] Both homogeneous and heterogeneous nucleation were observed during the transformation, and liquid phase, even in a small amount, can greatly accelerate the transformation. In the Y-α-β sialon composite, the following transformation is suggested:[39]

$$\alpha_1 + L \rightarrow \alpha_2 + \mathrm{YAG} \tag{6}$$

where α_2 has a lower x (here $x = m/3$) value than α_1. It is probable that the unbalanced oxidation of α and β sialon and stress induction drive the phase transformation. Because of the strong dependence of the creep on intergranular phase, phase transformation decreases the creep resistance of Y-α-β sialon composite, quantifying this behavior is not documented.

5. Conclusion

The four-point bending creep behavior of a Y-α-β sialon composite was investigated at temperatures of 1250–1350°C and stresses of 110–290 MPa. The results are:

1. At 1250, 1300 and l350°C, the stress exponents are 1.31±0.12, 1.49±0.15 and 1.62±0.10, respectively, and creep activation energy is 677±25 kJ mol^{-1}.
2. Microstructure observation indicates that most of cavities are formed at triple grain junctions.
3. Diffusion accommodated by grain boundary sliding is the dominant creep mechanism. The diffusion may be controlled by N^{3-} diffusing along the the grain boundary.
4. Because of the purification of intergranular phase, oxidation enhances the creep resistance of the composite.
5. Phase transformation results in the increase of the content of intergranular phase YAG and deteriorates the creep behavior of the composite.

Acknowledgements

This work was supported by the National Natural Science Foundation of China under grant 59772008. The authors are grateful to Dr. J.B. Ho for TEM and HREM observations, Mrs. J.H. Gao for SEM observations and Dr. W.W. Chen for useful discussions.

References

1. Schmid, H. and Rühle, M., Structure of special grain boundaries in sialon ceramics. *J. Mater. Sci.*, 1984, **19**, 615–628.
2. Cheng, Y. B. and Thompson, D. P., Preparation and grain boundary devitrification of Sm-α-sialon ceramics. *J. Eur. Ceram. Soc.*, 1994, **14**, 13–21.
3. Bernard-Granger, G., Crampon, J., Duclos, R. and Cales, B., High temperature creep behavior of β′-Si_3N_4/α sialon ceramics. *J. Eur. Ceram. Soc.*, 1997, **17**, 1647–1654.
4. Karunaratne, B. S. B. and Lewis, M. H. I., High-temperature fracture and diffusional deformation mechanisms in sialon ceramics. *J. Mater. Sci.*, 1980, **15**, 449–462.
5. Chen, C. F. and Chuang, T. Z., High temperature mechanical properties of sialon ceramic: creep characterization. *Ceram. Eng. Sci. Proc.*, 1987, **8**, 796–804.
6. Shiogai, T., Tsukamoto, K. and Sashida, N., Creep properties of (Si–Al–O–N) SC whisker composites. *J. Mater. Sci.*, 1998, **33**, 769–773.
7. Klemm, H., Herrmann, M., Reich, T., Schubert, C., Frassek, L., Wötting, G., Gugel, E. and Niefeld, G., High-temperature properties of a mixed α/β-sialon materials. *J. Am. Ceram. Soc.*, 1998, **81**, 1141–1148.
8. Wereszczak, A. A., Kirkland, T. P., Ferber, M. K., Watkins, T. R. and Yeckley, R. L., The effects of residual α phase on the 1370°C creep performance of yttria-doped HIPed silicon nitride. *J. Mater. Sci.*, 1998, **33**, 2053–2060.
9. Karunaratne, B. S. B. and Lewis, M. H., Grain boundary desegregation and intergranular cohesion in Si–Al–O–N ceramics. *J. Mater. Sci.*, 1980, **15**, 1781–1789.
10. Crampon, J., Duclos, R. and Rakotoharisoa, N., Creep behaviour of $Si_3N_4/Y_2O_3/A1_2O_3$/AlN alloys. *J. Mater. Sci.*, 1993, **28**, 909–916.
11. Wilkinson, D. S., Creep mechanisms in silicon nitride ceramics. In: *Tailoring of Mechanical Properties of Si_3N_4 Ceramics*, ed. M. J. Hoffmann and G. Petzow, Kluwer Academic Publishers, The Netherlands, pp. 327–338..
12. Wiederhorn, S. M., Luecke, W. E., Hockey, B. J. and Long, G. G., Creep Damage Mechanisms in Si_3N_4. In: *Tailoring of Mechanisms Properties of Si_3N_4 Ceramics*, ed. M. J. Hoffmann and G. Petzow, Kluwer Academic Publishers, The Netherlands, 1994, pp. 305–327.
13. Luecke, W. E., Wiederhorn, S. M., Hockey, B. J., Krause Jr., R. F. and Long, G. G., Cavitation contribute substatially to tensile creep in silicom nitride. *J. Am. Ceram. Soc.*, 1995, **78**, 2085–2096.
14. Crampon, J., Duclos, R., Peni, F., Guicciardi, S. and De Porte, G., Compressive creep and creep failure of $8Y_2O_3/3A1_2O_3$-doped hot pressed silicon nitride. *J. Am. Ceram. Soc.*, 1997, **80**, 85–91.
15. Cannon, R. M., Rhodes, W. H. and Heuer, A. H., Plastic deformation of fine-grained alumina (Al_2O_3): I interface-controlled diffusional creep. *J. Am. Ceram. Soc.*, 1980, **63**, 46–53.
16. Shi, J. L., Lu, Z. L., Gao, J. H., Zhu, G. Q., Li, L and Lai, T. R., Microstructure and micromechanical properties of Y-TZP and Y-TZP/$A1_2O_3$ composite after superplastic deformation. *Acta. Mater.*, 1998, **40**, 1923–1932.
17. Gazzara, C. P. and Messier, D. R., Determination of phase content of Si_3N_4 by X-ray. *Am. Ceram. Soc. Bull.*, 1977, **56**, 777–780.
18. Šajgalík, P., Hnatko, M., Lofaj, F., Hvizdoš, P., Dusza, J., Warbichler, P., Hofer, F., Riedel, R., Lecomte, E. and Hoffmann, M. J., SiC/Si_3N_4 nano/micro-composite-processing, RT and HT mechanical properties. *J. Eur. Ceram. Soc.*, 2000, **20**, 453–462.
19. Todd, J. A. and Xu, Z. Y., The high temperature creep deformation of Si_3N_4–$6Y_2O_3$–$2Al_2O_3$. *J. Mater. Sci.*, 1989, **24**, 4443–4452.
20. Xu, Y. R., Fu, X. R. and Yan, D. S., Creep behavior of hot-pressed silicon nitride ceramics with rare-earthed oxides and alumina additives. *Physica B*, 1988, **150**, 276–282.
21. Cinibulk, M. K., Thomas, G. and Johnson, S. M., Strength and creep behavior of rare-earthed disilicate-silicon nitride ceramics. *J. Am. Ceram. Soc.*, 1992, **75**, 2050–2055.
22. Chokshi, A. K. and Langdon, T. G., Characteristics of creep deformation in ceramics. *Mater. Sci. and Technol.*, 1991, **7**, 577–584.
23. Palm, J. A. and Greskovich, C. D., Thermomechanical properties of hot-pressed $S1_{2.9}Be_{0.1}N_{3.8}O_{0.2}$. *Am. Ceram. Soc. Bull.*, 1980, **59**, 447–452.
24. Bouarroudj, A., Goursat, P. and Besson, J. L., Oxidation resistance and creep behavior of a silicon nitride ceramic densified with Y_2O_3. *J. Mater. Sci.*, 1985, **20**, 1150–1159.
25. Raj, R. and Morgan, P. E. D., Activation energies for densification, creep, and grain boundary Sliding in nitrogen ceramics. *J. Am. Ceram. Soc.*, 1981, **64**, C143–C145.
26. Stevens, R. N., Grain boundary sliding and diffusion creep in polycrystalline solids. *Phil. Mag.*, 1971, **23**, 265–283.
27. Ferber, M. K. and Jenkins, M. G., Evaluation of the strength and creep-fatigue behaviour of a hot isostatically pressed silicon nitride. *J. Am. Ceram. Soc.*, 1992, **75**, 2453–2462.
28. Ohji, T. and Yamauchi, Y., Tensile creep and creep rupture of monolithic and SiC-whisker-reinforced silicon nitride ceramics. *J. Am. Ceram. Soc.*, 1993, **76**, 3105–3112.
29. Evans, A. G. and Rana, A., High temperature failure mechanisms in ceramics. *Acta. Metall.*, 1980, **28**, 129–141.
30. Tsai, R. L. and Raj, R., Creep fracture in ceramics containing small amounts of liquid phase. *Acta. Metall.*, 1982, **30**, 1043–1058.
31. Monkman, F. C. and Grant, N. J., An empirical relationship between rupture life and minimum creep rate in creep–rupture tests. *Proc. Am. Soc. Test. Mater.*, 1956, **56**, 593–620.
32. Lewis, M. H. and Barnard, P., Oxidation mechanisms in Si–Al–O–N ceramics. *J. Mater. Sci.*, 1980, **15**, 443–448.
33. Cinibulk, M. K., Thomas, G. and Johnson, S. M., Oxidation behavior of rare-earth disilicate-silicon nitride ceramics. *J. Am. Ceram. Soc.*, 1992, **75**, 2044–2049.
34. Komeya, K., Haruna, Y., Meguro, T., Kameda, T. and Asayama, M., Oxidation behavior of the sintered Si_3N_4–Y_2O_3–Al_2O_3 system. *J. Mater. Sci.*, 1992, **27**, 5727–5734.
35. Ramesh, R., Byrne, P., Hampshire, S. and Pomeroy, M. J., Kenetics of weight changes and morphological developments during oxidation of pressureless sintered β-sialons. *J. Eur. Ceram. Soc.*, 1997, **17**, 1901–1909.
36. Nordberg, L.-O., Nygren, M., Käll, P.-O. and Shen, Z., Stability and oxidation properties of Re-alpha-sialon ceramics (Re = Y, Nd, Sm, Yb). *J. Am. Ceram. Soc.*, 1998, **81**, 1461–1470.
37. Mieskowski, D. M. and Sanders, W. A., Oxidation of Si_3N_4 sintered with rare-earth oxides additions. *J. Am. Ceram. Soc.*, 1985, **68**, C–l60–C-163.
38. Kijima, K. and Shirasaki, S., Nitrogen self-diffusion in silicon nitride. *J. Chem. Phys.*, 1976, **65**, 2668–2671.
39. Falk, L. K. L., Shen, Z. and Ekström, T., Microstructural stability of duplex α-β sialon ceramics. *J. Eur. Ceram. Soc.*, 1997, **17**, 1099–1112.